Biosensors and Bioelectronics 95 (2017) 48–54

Contents lists available at ScienceDirect

Biosensors and Bioelectronics

journal homepage: www.elsevier.com/locate/bios

Gold nanoparticle-based low limit of detection Love wave biosensor for carcinoembryonic antigens

Shuangming Li[a,b], Ying Wan[a], Yan Su[a], Chunhai Fan[a], Venkat R. Bhethanabotla[b,*]

[a] School of Mechanical Engineering, Nanjing University of Science and Technology, Nanjing, China
[b] Department of Chemical & Biomedical Engineering, University of South Florida, Tampa, Florida, USA

ARTICLE INFO

Keywords:
Surface acoustic wave
Love wave
Biosensors
CEA
Gold nanoparticles

ABSTRACT

In this work, a Love wave biosensing platform is described for detecting cancer-related biomarker carcinoembryonic antigen (CEA). An ST 90°-X quartz Love wave device with a layer of SiO_2 waveguide was combined with gold nanoparticles (Au NPs) to amplify the mass loading effect of the acoustic wave sensor to achieve a limit of detection of 37 pg/mL. The strategy involves modifying the Au NPs with anti-CEA antibody conjugates to form nanoprobes in a sandwich immunoassay. The unamplified detection limit of the Love wave biosensor is 9.4 ng/mL. This 2–3 order of magnitude reduction in the limit of detection brings the SAW platform into the range useful for clinical diagnosis. Measurement electronics and microfluidics are easily constructed for acoustic wave biosensors, such as the Love wave device described here, allowing for robust platforms for point of care applications for cancer biomarkers in general.

1. Introduction

Accurate quantification of cancer biomarkers is critical for early diagnosis and monitoring. However, these trace protein biomarkers, such as CEA, CA125 and Bcl-2, are present in a very low concentration level in serum or urine of cancer patients (Anderson et al., 2009; Drenberg et al., 2010; Ni et al., 2005). Traditional assay methods such as enzyme-linked immunosorbent assay (ELISA) (Butler, 2000), radioimmunoassay (Kato and Torigoe, 1977), fluorescence immunoassay (Hicks, 1984), electrophoretic immunoassay (Liu et al., 2008) and mass spectrometric immunoassay (Nelson et al., 1995) have some disadvantages, such as requiring labeled markers, long processing times and requiring expensive instruments. Thus, the demand for rapid, operationally simple, ultrasensitive biosensors is increasing, especially those capable of point of care use.

Surface acoustic wave (SAW) biosensors have been used in biological application for many years (Länge et al., 2008). SAW biosensors have the advantages of high sensitivity, small dimension, low cost, and can be used in label-free and real-time monitoring. They therefore have great potential in clinical diagnosis, especially in point of care testing and portable sensing applications (Hur et al., 2005; Länge et al., 2003). The SAW sensor is a piezoelectric mass sensor that can be sensitive to mass loading on the surface, as the loading can influence the propagation of the acoustic wave (Ballantine et al., 1997). Amongst various SAW sensors, Love wave sensor, also named guided shear horizontal SAW sensor, is a favored device for liquid phase applications. This device has a low velocity waveguide layer on a piezoelectric oxide surface in which shear horizontal SAWs are propagated using suitably designed and lithographically patterned interdigital transducers (IDT). The waveguide layer reduces power consumption and increases sensitivity (Gaso et al., 2013). Though the Love wave sensor has a much higher sensitivity than other piezoelectric sensors, such as quartz crystal microbalances (Gaso et al., 2013; Ward and Buttry, 1990; Zhang et al., 2015), its limit of detection for practically useful devices is not low enough to quantify cancer biomarkers at the required pg/mL levels (Anderson et al., 2009).

Nanoparticle-biomolecule hybrid materials have been studied and utilized in biomedical applications recently (Azzazy et al., 2006; Grodzinski et al., 2006). Owing to the unique electronic, photonic, catalytic properties and dimensional similarity, the integration of nanoparticles with biomolecules (e.g. DNA and proteins) leads to novel synergetic functionalized hybrid nanobiomaterials. With the aim of lower limit of detection, various signal amplification strategies based on nanoparticle-biomaterials have been developed. Amongst these, gold nanoparticles (Au NPs) have been studied and used because of numerous advantages, such as good compatibility with biomolecules and high surface-to-volume ratio (Daniel and Astruc, 2004). Au NPs can increase the sensitivity in various ways, such as through the loading of large amounts of electroactive labels in electrochemical immunosensing (Das et al., 2006; Mani et al., 2009), and heavy mass loading in

* Corresponding author.
E-mail address: bhethana@usf.edu (V.R. Bhethanabotla).

http://dx.doi.org/10.1016/j.bios.2017.04.012
Received 23 December 2016; Received in revised form 28 March 2017; Accepted 11 April 2017
Available online 12 April 2017

mass immunosensing (Chu et al., 2012; Ma et al., 2002). For example, Dequaire et al. developed a sensitive electrochemical immunoassay using a colloidal gold label that was indirectly determined by anodic stripping voltammetry (ASV) at a single-use carbon-based screen-printed electrode (SPE). This method was evaluated for a noncompetitive heterogeneous immunoassay of an immunoglobulin G (IgG) and a concentration as low as 3×10^{-12} M was determined (Dequaire et al., 2000). He et al. reported a new approach to ultrasensitive detection of DNA hybridization based on nanoparticle-amplified surface plasmon resonance (SPR). They observed a 2–4 order of magnitude improvement in sensitivity compared with literature values for unamplified scanning (He et al., 2000).

In this work, we present a sensitive carcinoembryonic antigen (CEA) detection strategy based on an Au NP-amplified immunoassay with a Love wave biosensor. CEA is a glycosylphosphatidylinositol cell surface anchored glycoprotein that is a well-known, broad spectrum biomarker related to various cancers (Moertel et al., 1993; Wiggers et al., 1986), and it is also an indicator of disease recurrence (Wanebo et al., 1978). In our previous work, the design and fabrication of various SAW sensors has been presented (Li et al., 2015; Richardson et al., 2015). The orientation of the crystal relative to the propagation direction is an important factor; different cut angles lead to different values for the acoustic velocity, coupling coefficient (K^2), and temperature coefficient of frequency (TCF). Thus, the choice of the crystal orientation becomes a very critical factor. In biosensing applications, the liquid has a large damping effect on the particle movement in the direction normal to the surface, which leads to larger power consumption, therefore, the particle displacement must be polarized in the shear-horizontal direction (Moriizumi et al., 1987). Common choices for piezoelectric substrates to construct Love wave biosensor devices are ST-X quartz and 36° Y-cut lithium tantalate ($LiTaO_3$) (Bender et al., 2000; Schlensog et al., 2004). Besides the advantages of stability, easy integration and low cost, we found that ST quartz SAW devices can combine sample mixing and non-specific binding removal functions, showing potential for future point of care and portable diagnosis applications (Morrill, 2014). Thus, a sensor with a center frequency of about 120 MHz was fabricated in ST-90 ° quartz with a SiO_2 waveguide layer for this work. To achieve a low limit of detection, a sandwich assay with anti-CEA antibody assembled with Au NPs is conceived. The fabricated biosensors were tested with and without the Au NP nanoprobes for CEA quantification at clinically relevant levels of tens of picograms per milliliter.

2. Experimental

2.1. Materials and methods

Carcinoembryonic antigen full length protein was purchased from Adcam (MA,USA). Mouse monoclonal capture CEA antibody (CEA mAb, clone no. M11147) and mouse monoclonal detection CEA antibody (CEA mAb, clone no. M11146) were purchased from Fitzgerald (MA, USA). Gold(III) chloride trihydrate ($HAuCl_4{\cdot}3H_2O$, 99.9+%), lyophilized 99% bovine serum albumin (BSA), terephthalaldehyde ($C_8H_6O_2$, 99%) and polyethylene oxide (PEG2000) were purchased from Sigma-Aldrich (WI, USA). Citric acid, trisodium salt dihydrate ($C_6H_5Na_3O_7{\cdot}2H_2O$, 99%) and aminopropyltriethoxy-silane (APTES, 99%) were purchased from Acros Organics (NJ, USA). Immunoreagents were dissolved in pH 7.4, 0.1 M phosphate buffered saline (PBS) (0.01 M phosphate, 0.14 M NaCl, 2.7 mM KCl).

2.2. Gold nanoparticle synthesis

Au NPs were synthesized via an adaptation of the well-established Frens and Turkevich method (Frens, 1973; Kimling et al., 2006). In this work, an inverse-order method was used. By exchanging the order of reagent addition, it is possible to increase the oxidation rate of sodium citrate and hence control the size and morphology, with a narrower size distribution than the standard Turkevich approach (Ojea-Jiménez et al., 2011). Narrow size distribution of the Au NPs is important for reproducibility and repeatability of the sensor responses. If particle distribution were not controlled, nanoparticle samples taken for different sensor determinations could have slightly different particle size distributions, and they could distribute differently on the surface of the SAW device as well. While the mass loading effect of the SAW device response is targeted for this application, viscoelastic properties of the adhered material also affect device response. A narrow distribution of the Au NPs will minimize these effects on the sensor response and contribute towards reproducible and repeatable sensor responses. The molar ratio of sodium citrate/$HAuCl_4$ is 6.8. Initially 25 mL of ultrapure (Milli-Q) water was heated up to 90 °C in an oil bath and then, 2.5 mL of 10.35 mg/mL sodium citrate was added. After the temperature of the solution was constant again, 1 mL of 5 mg/mL aqueous solution $HAuCl_4{\cdot}3H_2O$ was added and continuously heated for 15 min before cooling down to room temperature using an ice bath.

The optical absorption spectra of the gold colloidal solutions were measured using a Perkin Elmer Lambda 35 UV/Vis spectrophotometer (Perkin Elmer, USA). Dynamic light scattering (DLS) was performed on Zetasizer Nano ZS90 (Malvern, UK) to measure the average diameter of gold particles. The morphology of the synthesized gold particles was characterized by scanning electron microscopy (SEM, Hitachi S-800, Japan). An Agilent 8753ES network analyzer (Agilent, USA) was used to measure the SAW device responses. A syringe pump (Harvard Apparatus PHD 22/2000, USA) was used for the sample injection.

2.3. Preparation of the nanoprobes

The optimal dose of antibody for coating the gold particles were established first. Insufficient ratio of antibodies to colloidal gold particles could lead to instability, with consequent aggregation of the gold particles, which can be seen from the color change. The colloidal gold solution was first adjusted to pH 9 by adding 100 mM Na_2CO_3, and separated into 4 cells of 200 μL each. 1 mg/mL detection anti-CEA antibody solutions was added to each cell with varying volumes. After 5 min, 10 μL of 10% NaCl solution was added to each cell, and 1 min later, the color change of each cell was observed. The solution color in cell with 1 μL and 2 μL antibody turned from red to violet and the ones with 5 μL and 10 μL antibody solutions remained red. Thus, 5 μL/200 μL was determined to be the optimal ratio of antibody solution to colloidal gold solution. The results for different assembly ratios are shown in the Supplementary material.

After the optimal ratio was determined, the Au NPs were modified with detection anti-CEA antibody to prepare the nanoprobe conjugates as follows: 1 mL of colloidal gold solution was centrifuged and the supernatant was removed to concentrate the solution to 200 μL. After mixing, 100 mM Na_2CO_3 was added to the solution to adjust the pH of the solution to 9. Then, 25 μL of 1 mg/mL detection anti-CEA antibody was added and stored overnight at 4 °C after shaking for 20 min. In the next step, 5% PEG2000 was mixed with the assembled solution to reach a concentration of 0.5%, and stored for 1 h at 4 °C. To remove the excess antibodies, the gold nanoprobe solution was centrifuged, supernatant-removed and re-suspended with 500 μL of 0.1 mM phosphate buffered saline (PBS, pH 7.4) with 1% BSA, which was repeated 3 times. Finally, the nanoprobe solution were stored at 4 °C prior to further use.

2.4. Love wave sensor design and fabrication

Owing to the outstanding temperature performance and processing ease for ST-quartz compared to other piezoelectric crystals such as $LiTaO_3$ and $LiNbO_3$ (Zhou et al., 2013), and also the potential for

combining sample mixing and non-specific binding removal functions (Morrill, 2014), we choose ST-cut quartz as the substrate material in this work. A waveguide layer has traditionally been employed for enhancing acoustic energy confinement near the surface and is known to be beneficial in improving SAW device performance. Typically, SiO_2 and polymers such as poly(methyl methacrylate) (PMMA) have been used to construct the waveguide layer for Love wave sensors (Branch and Brozik, 2004; Du et al., 1996). Polymers, though having low density and low shear velocity, are usually lossy, and with increasing thickness, the acoustic wave absorption increases rapidly (Gizeli et al., 2003). Compared with the polymers, SiO_2 is more chemically stable and resistant to degradation. Thus, in this work, we chose SiO_2 as the waveguide material (Ballantine et al., 1997; Li et al., 2017).

The 120 MHz Love wave devices were fabricated on 500 μm thickness 4-in. ST-X cut quartz single-side polished wafers. The input and output IDT electrodes of each sensor consisted of 60 finger pairs with an electrode width of 10 μm and wavelength of 40 μm. The delay line is of 8 mm length and 2 mm width. The IDT patterns were fabricated by the following steps: First, NR9 1500PY (Futurrex) negative photoresist was applied by spin coating on the wafer after solvent cleaning. After the pre-bake, the coated wafer was exposed to broadband UV light using EVG mask aligner, followed by a hard bake. The pattern was developed in RD6 (Futurrex) developer for 12 s, followed by rinsing with DI water and drying with nitrogen gas. E-beam evaporation was used to deposit 20 nm/100 nm Ti/Au adhesion and metal layers. The deposition rate was set to 0.5 nm/s for Ti deposition and 1 nm/s for Au to obtain strong adhesion between the substrate and metal layer. An acetone bath was used to lift-off the metal and the remaining metal pieces were removed with solvent cleaning, with ultrasonication used as needed to achieve complete cleaning. After the metal IDT patterns were fabricated, the open contact pads were protected with Kapton tape before SiO_2 deposition. Using plasma enhanced chemical vapor deposition (PECVD), a 1 μm thick SiO_2 waveguide layer was deposited on the surface of the SAW devices. The patterned wafers were finally diced into 20 mm×20 mm individual chips (Fig. 1a).

2.5. Sensing chip and microfluidic system

An SU-8 photoresist mold was designed on a silicon wafer to fabricate the polydimethylsiloxane (PDMS) microchannels for the SAW chips (Fig. 1b). The chip has a chamber above the delay path and two air chambers to protect the IDTs, in case of high energy consumption. The PDMS liquid (Sylgard 184 silicone elastomer kit) was mixed with a crosslinking rate 1:10 and injected on the top of the mold. After heating at 125 °C in an oven for 20 min, the PDMS solution was cross-linked to a solid, and striped off from the mold. The molded PDMS material was diced into individual microchannel cells, punched and chemically bonded with the SAW chips using O_2 plasma treatment (Fig. 1c). A schematic diagram of the complete sensor is shown in Fig. 1d.

The injection pump was set at a flow rate of 10 μL/min and a Y-type joint was used to switch channels between the buffer and sample solutions. The mass loading on the SAW sensor was monitored by tracking the phase shift of the device at center frequency via the network analyzer sending the data to the computer.

2.6. Surface preparation of the SAW device

The surface of the SAW device was solvent cleaned and treated by O_2 plasma, after the PDMS bonding (Fig. 2a). The SiO_2 waveguide layer was soaked in 10 mM APTES in pure ethyl alcohol for at least 30 min. After rinsing with pure ethyl alcohol and drying by N_2 gas repeated 3 times, the SAW device was baked in an oven at 110 °C for 30 min (Fig. 2b). After the device cooled down to room temperature, the SiO_2 waveguide layer was soaked in 10 mM terephthalaldehyde in pure acetone for at least 30 min, followed by pure water rinsing and N_2 gas drying (Fig. 2c).

100 μg/mL capture anti-CEA antibody was assembled on the surface of the SAW device and stored overnight. Then 1% BSA solution in PBS was used to block the non-sensing surface (treatment time was at least one hour), then rinsed with PBS and dried using N_2 gas. The modified SAW biosensor was stored at 4 °C (Fig. 2d).

3. Results and discussion

3.1. Characterization of the nanoparticles

The nanoparticle size was measured by DLS. Fig. 3a shows that the gold particle size distribution is in a narrow range, with 81.7% of the particles' sizes within 10 nm~16 nm and a single peak at 11.7 nm. The synthesized gold particles were visualized with SEM (Fig. 3b) and most had a spherical morphology.

The optical absorption of the colloidal gold solutions before and after the antibodies assembled with the particles is compared in Fig. 3c. The synthesized colloidal gold solution had a plasmon absorbance maximum at a wavelength of 519 nm. The absorbance peak near 519 nm is typical of gold nanoparticles with average diameter in range of 10–15 nm, which is in agreement with the DLS analysis (Haiss et al.,

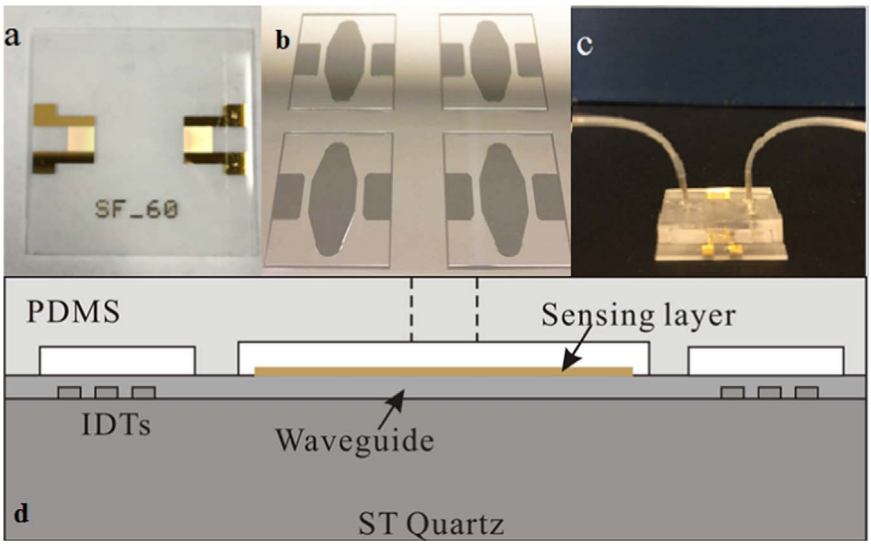

Fig. 1. a) Love wave chip; b) SU-8 photoresist mold on silicon wafer; c) PDMS microfluidic chip; d) Schematic diagram of the complete sensor.

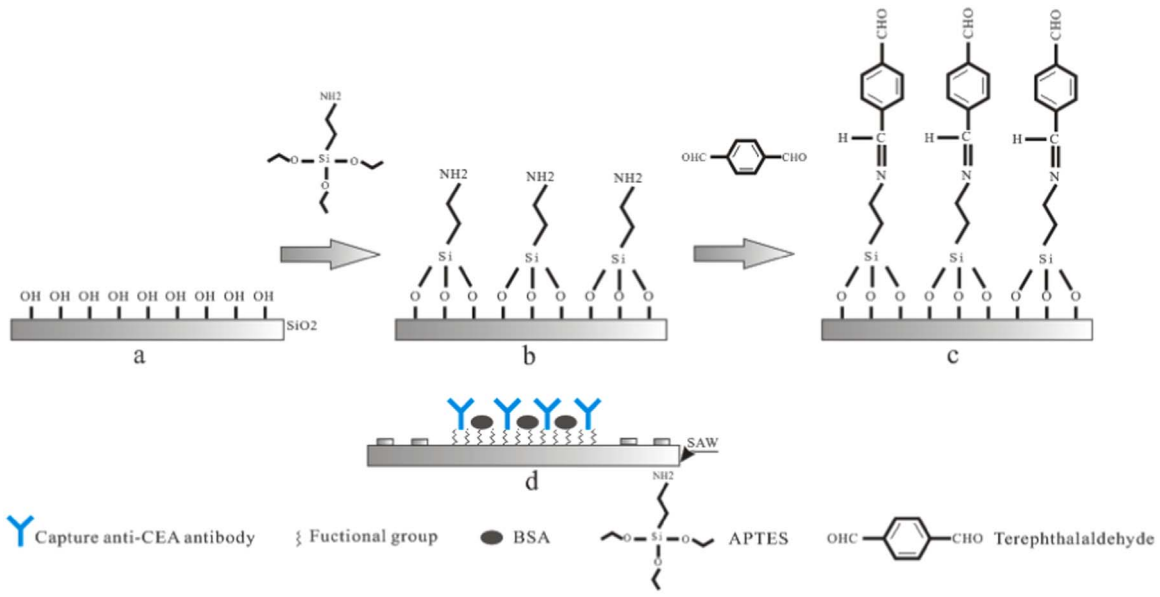

Fig. 2. Processing steps of surface modification: a) hydroxylation using O_2 plasma; b) silanization using APTES; c) hydroformylation using terephthalaldehyde; d) assembling caputure anti-CAE antibody and BSA on the suface.

2007; Link and El-Sayed, 1999). It was revealed that the antibody-assembled Au NP solutions before and after excess antibody process had plasmon absorbance peaks at 520 and 521 nm, respectively. The slight red-shift is due to the coating of proteins on the surface of the Au NPs. A high absorbance at the long wavelength region can be observed, owing to the aggregation of some particles during the removal of excess antibodies, repeated three times.

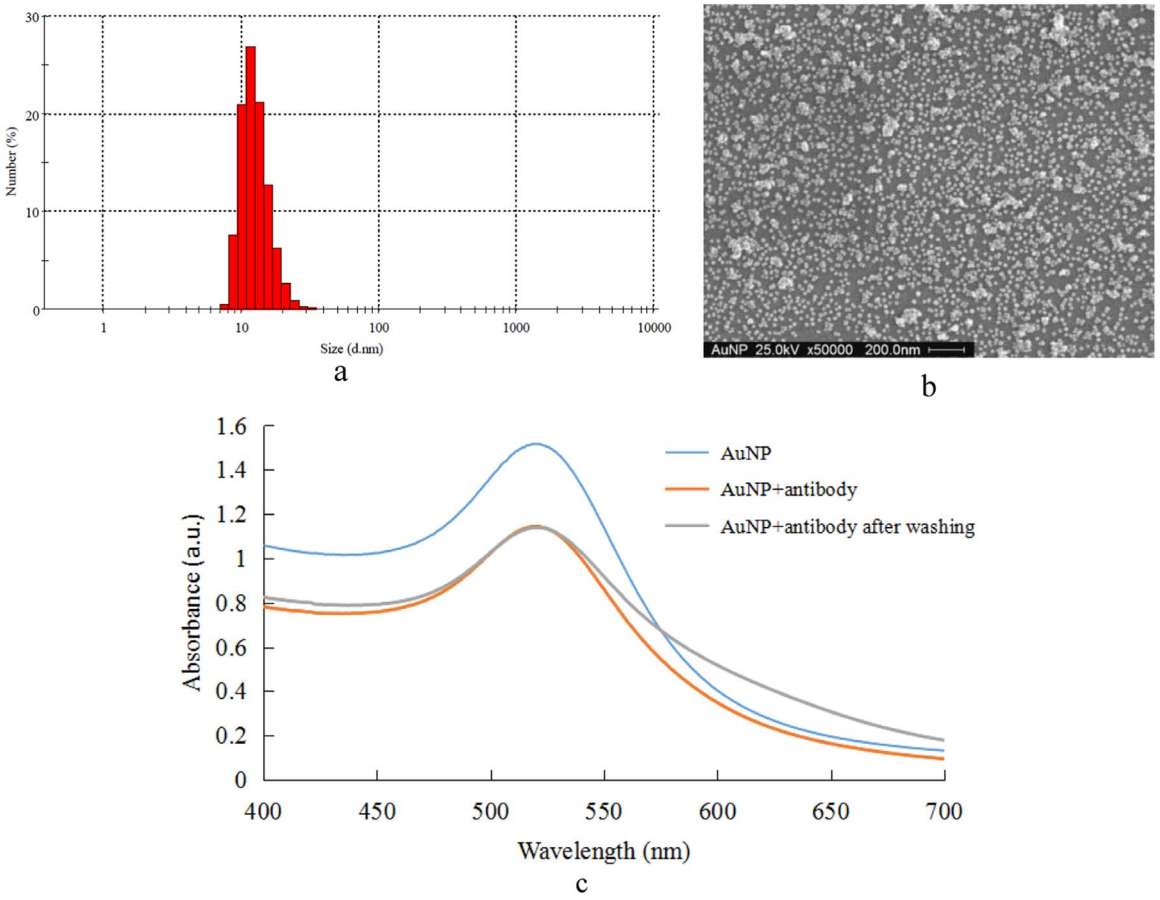

Fig. 3. a) Particle size distribution measured by DLS, the single peak is at 11.7 nm. b) Image of Au NPs under SEM; the magnification is 50,000x. c) UV–Vis absorption spectra of the Au NPs and assembled Au NPs solutions. The synthesized Au NP solution, assembled Au NP solution and assembled Au NP solution after 3 times washing show slightly different plasmon absorbance peaks at 519 nm, 520 nm and 521 nm, respectively.

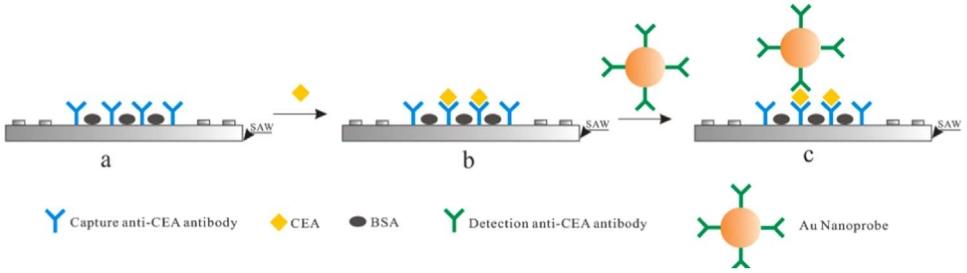

Fig. 4. CEA detection strategy; a) capture anti-CEA antibody modified surface; b) directly capturing the CEA molecules; c) using nanoprobe conjugates for amplifying the mass loading.

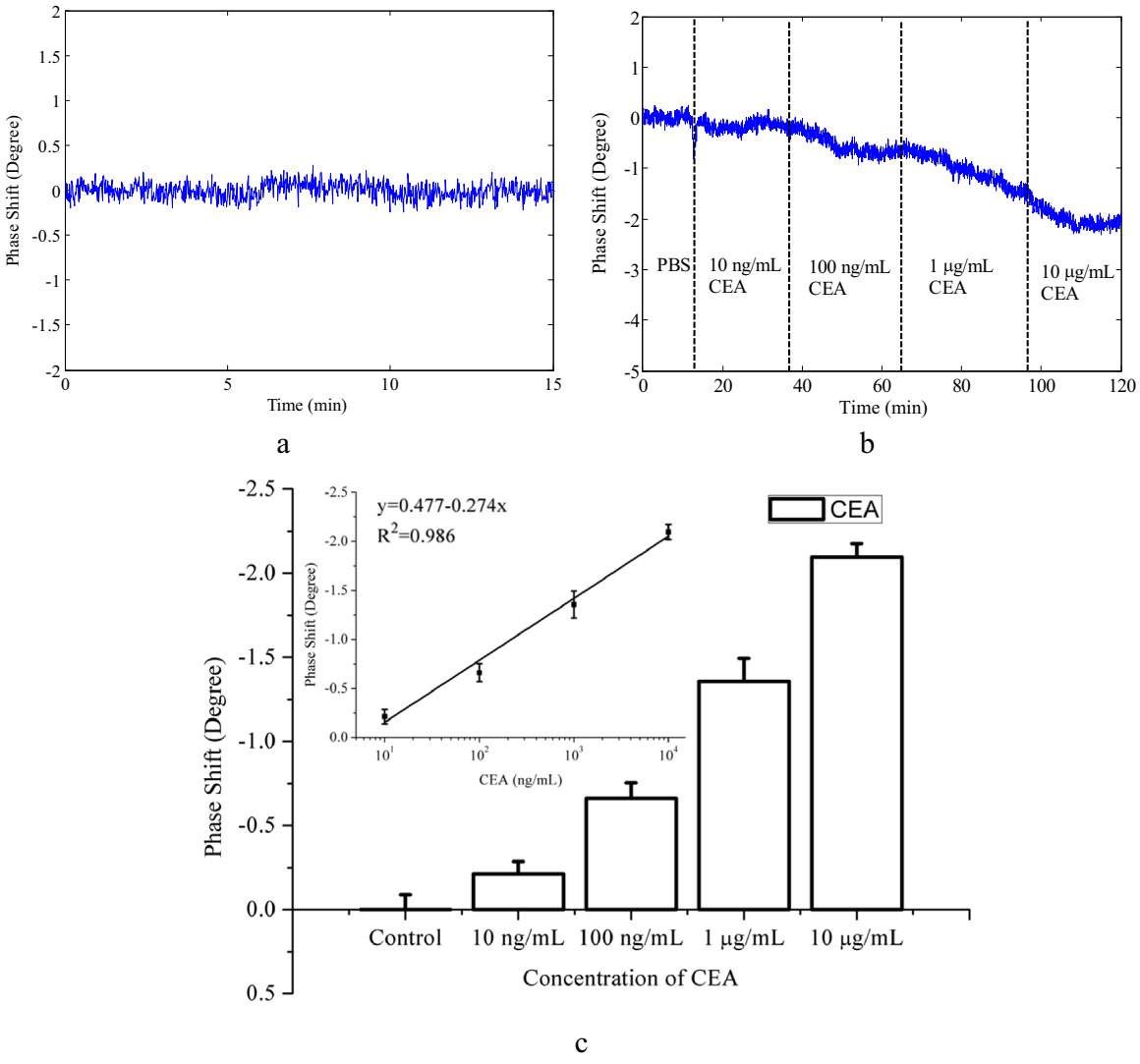

Fig. 5. Direct immunoassay results: a) baseline signal in PBS solution, the standard deviation is 0.089°; b) real-time response of detecting CEA with a series of concentrations from 10 ng/mL to 10 μg/mL; c) calibration curve for logarithmic concentration of target CEA.

3.2. Detection strategy

The two strategies utilized in SAW immunodetection are illustrated in Fig. 4. In the direct immunoassay, capture anti-CEA antibodies are assembled on the SAW surface to specifically bind with CEAs (Fig. 4a and b). A sandwich immunoassay was used here for the gold nanoprobe amplification (Fig. 4c). The nanoprobes were added after the CEAs were captured. The gold nanoprobes containing detection anti-CEA antibodies can also specifically bind with CEAs. Thus, the use of the nanoprobes can magnify the mass loading on the sensor surface, and enhance the sensitivity of the immunosensor.

3.3. Sensor response for CEA immunoassay

The real-time phase changes during the sensing process were measured by the detecting system. The sensor response with direct immunoassay is plotted in Fig. 5. The background noise level (σ=0.089°) was obtained by flowing PBS over the sensor chip before sample introduction, and the relatively stable baseline is shown in Fig. 5a. After 15 min, the CEA sample solution was injected. The phase angle began to decrease slightly due to the capture of CEA, and a steady phase was reached after 20 min. As the concentration increased, the phase angle of the sensor dropped further (Fig. 5b). The final phase

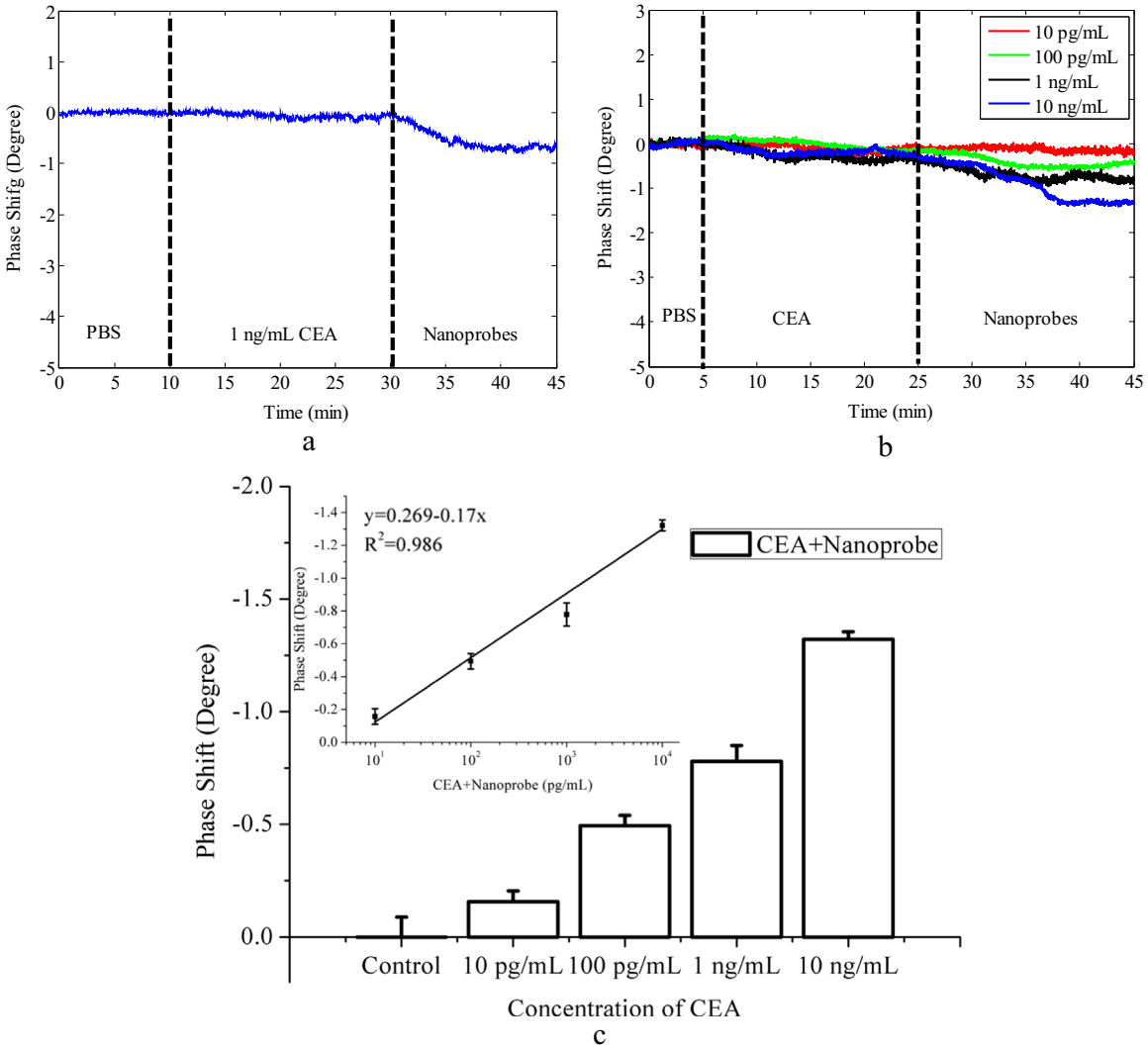

Fig. 6. Au NP amplified sandwich immunoassay results: a) real-time response of 1 ng/mL CEA; b) real-time response of CEA with a series of concentrations from 10 pg/mL to 10 ng/mL; c) calibration curve for logarithmic concentration of target CEA.

shift after 10 μg/mL CEA injection was 2.1°. The calibration curve for the CEA direct immunoassay is shown in Fig. 5c. In the detection of CEA, the relative phase change increased with the CEA concentration and was logarithmically related to the target concentration in the range of 10–10000 ng/mL. The limit of detection (LOD) for this direct immunoassay is established as 9.4 ng/mL using the formula:

$$LOD = \frac{3 \times \sigma}{Sensitivity} \quad (1)$$

The real-time response of Au NP amplified sandwich immunoassay is shown in Fig. 6. As shown in Fig. 6a, 1 ng/mL CEA was injected after the PBS injection. The CEA specifically binds with the capture anti-CEA antibody in the following 20 min. However, no significant phase change was observed, because the target concentration is much lower than the sensor's limit of detection. The nanoprobes assembled with detection anti-CEA antibody were added at 30 min. The phase dropped immediately and stabilized after about 20 min. The final phase shift was about 0.7°. The detecting result confirmed that the nanoprobe conjugates amplified the mass loading successfully. Varying concentrations, from 10 pg/mL to 10 ng/mL, of CEA samples were measured, and the real-time data are plotted in Fig. 6b. During the CEA injection period, the phase shift was not significant. When the nanoprobes were added, the phase difference became significant. The higher the concentration of CEA solution was, the faster and larger the phase dropped. After 20 min of binding, the phase shifts were stable and can be clearly distinguished in each curve. Fig. 6c shows the calibration curve of the nanoprobe amplified immunoassay. The relative phase change increased with the CEA concentration and is logarithmically related to the target concentration in the range of 10 pg/mL to 10 ng/mL. As a result, the limit of detection was established as 37 pg/mL for the sandwich immunoassay. The regression coefficient (R^2) is 0.986. Compared with the direct immunoassay, this Au NP amplified assay had a greater-than 250-fold lower limit of detection. Table 1 shows this sensor has outstanding performance in terms of level of detection when compared with many recent sensors reported in the literature.

Table 1
Comparison of the LOD with literature.

Literature	Type	Target	LOD	R^2
Rupp et al. (2008)	SH-SAW	IgG	4 μg/mL	–
Onen et al. (2012)	Love wave	Bcl–2	0.5 ng/mL	0.959
Jiang et al. (2015)	Love wave	H1N1 HA	1 ng/mL	–
Hur et al. (2005)	SH-SAW	DNA	> 10 ng/mL	–
This work	Love wave	CEA	37 pg/mL	0.986

4. Summary and conclusions

In summary, we report a surface acoustic wave-based CEA immunodetection platform. A Au NP amplified assay is developed to lower the limit of detection by 2–3 orders of magnitude. By combining Au NP based nanoprobes with a Love wave biosensor, quantification of CEA in the clinically relevant range is demonstrated. The new nanoprobe strategy was compared with the direct detection method using the Love wave device and advantages in level of detection were demonstrated. Assays for quantification of other cancer biomarkers in low, clinically relevant concentrations can be developed using the principles presented in this work. The SAW platform is robust and can be configured in point of care formats for rapid quantification of biological cancer markers at low concentrations.

Acknowledgments

This work was financially supported by the National Science Foundation grant number IIP-1640668 and China National Science Foundation grant numbers 61371039 and 21105048, which is gratefully acknowledged.

Appendix A. Supplementary material

Supplementary data associated with this article can be found in the online version at doi:10.1016/j.bios.2017.04.012.

References

Anderson, N.S., Bermudez, Y., Badgwell, D., Chen, R., Nicosia, S.V., Bast, R.C., Jr, Kruk, P.A., 2009. Urinary levels of Bcl-2 are elevated in ovarian cancer patients. Gynecol. Oncol. 112 (1), 60–67.

Azzazy, H.M.E., Mansour, M.M.H., Kazmierczak, S.C., 2006. Nanodiagnostics: a new frontier for clinical laboratory medicine. Clin. Chem. 52 (7), 1238.

Ballantine, D.S., White, R.M., Martin, S.J., Ricco, A.J., Zellers, E.T., Frye, G.C., Wohltjen, H., 1997. Acoustic wave sensors: theory, design, and physico-chemical applications. Academic Press.

Bender, F., Cernosek, R.W., Josse, F., 2000. Love-wave biosensors using cross-linked polymer waveguides on $LiTaO_3$ substrates. Electron. Lett. 36 (19), 1672–1673.

Branch, D.W., Brozik, S.M., 2004. Low-level detection of a Bacillus anthracis simulant using Love-wave biosensors on 36° YX $LiTaO_3$. Biosens. Bioelectron. 19 (8), 849–859.

Butler, J.E., 2000. Enzyme-linked immunosorbent assay. J. Immunoass. 21 (2–3), 165–209.

Chu, P.-T., Lin, C.-S., Chen, W.-J., Chen, C.-F., Wen, H.-W., 2012. Detection of gliadin in foods using a quartz crystal microbalance biosensor that incorporates gold nanoparticles. J. Agric. Food Chem. 60 (26), 6483–6492.

Daniel, M.-C., Astruc, D., 2004. Gold nanoparticles: assembly, supramolecular chemistry, quantum-size-related properties, and applications toward biology, catalysis, and nanotechnology. Chem. Rev. 104 (1), 293–346.

Das, J., Aziz, M.A., Yang, H., 2006. A nanocatalyst-based assay for proteins: dna-free ultrasensitive electrochemical detection using catalytic reduction of p-nitrophenol by gold-nanoparticle labels. J. Am. Chem. Soc. 128 (50), 16022–16023.

Dequaire, M., Degrand, C., Limoges, B., 2000. An electrochemical metalloimmunoassay based on a colloidal gold label. Anal. Chem. 72 (22), 5521–5528.

Drenberg, C.D., Saunders, B.O., Wilbanks, G.D., Chen, R., Nicosia, R.F., Kruk, P.A., Nicosia, S.V., 2010. Urinary angiostatin levels are elevated in patients with epithelial ovarian cancer. Gynecol. Oncol. 117 (1), 117–124.

Du, J., Harding, G.L., Ogilvy, J.A., Dencher, P.R., Lake, M., 1996. A study of Love-wave acoustic sensors. Sens. Actuators A: Phys. 56 (3), 211–219.

Frens, G., 1973. Controlled nucleation for the regulation of the particle size in monodisperse gold suspensions. Nature 241 (105), 20–22.

Gaso, M.I.R., Jiménez, Y., Francis, L.A., Arnau, A., 2013. Love Wave Biosensors: A Review. State of the Art in Biosensors—General Aspects, 277-310, InTech.

Gizeli, E., Bender, F., Rasmusson, A., Saha, K., Josse, F., Cernosek, R., 2003. Sensitivity of the acoustic waveguide biosensor to protein binding as a function of the waveguide properties. Biosens. Bioelectron. 18 (11), 1399–1406.

Grodzinski, P., Silver, M., Molnar, L.K., 2006. Nanotechnology for cancer diagnostics: promises and challenges. Expert Rev. Mol. Diagn. 6 (3), 307–318.

Haiss, W., Thanh, N.T.K., Aveyard, J., Fernig, D.G., 2007. Determination of size and concentration of gold nanoparticles from UV–vis spectra. Anal. Chem. 79 (11), 4215–4221.

He, L., Musick, M.D., Nicewarner, S.R., Salinas, F.G., Benkovic, S.J., Natan, M.J., Keating, C.D., 2000. Colloidal Au-enhanced surface plasmon resonance for ultrasensitive detection of DNA hybridization. J. Am. Chem. Soc. 122 (38), 9071–9077.

Hicks, J.M., 1984. Fluorescence immunoassay. Human. Pathol. 15 (2), 112–116.

Hur, Y., Han, J., Seon, J., Pak, Y.E., Roh, Y., 2005. Development of an SH-SAW sensor for the detection of DNA hybridization. Sens. Actuators A: Phys. 120 (2), 462–467.

Jiang, Y., Tan, C.Y., Tan, S.Y., Wong, M.S.F., Chen, Y.F., Zhang, L., Yao, K., Gan, S.K.E., Verma, C., Tan, Y.-J., 2015. SAW sensor for Influenza A virus detection enabled with efficient surface functionalization. Sens. Actuators B: Chem. 209, 78–84.

Kato, H., Torigoe, T., 1977. Radioimmunoassay for tumor antigen of human cervical squamous cell carcinoma. Cancer 40 (4), 1621–1628.

Kimling, J., Maier, M., Okenve, B., Kotaidis, V., Ballot, H., Plech, A., 2006. Turkevich method for gold nanoparticle synthesis revisited. J. Phys. Chem. B 110 (32), 15700–15707.

Länge, K., Bender, F., Voigt, A., Gao, H., Rapp, M., 2003. A surface acoustic wave biosensor concept with low flow cell volumes for label-free detection. Anal. Chem. 75 (20), 5561–5566.

Länge, K., Rapp, B.E., Rapp, M., 2008. Surface acoustic wave biosensors: a review. Anal. Bioanal. Chem. 391 (5), 1509–1519.

Li, S., Richardson, M., Sankaranarayanan, S.K., Fan, C., Su, Y., Bhethanabotla, V.R., 2015. Design and fabrication of SiO_2 waveguide-based SAW sensors with filled microcavities. SENSORS, 2015, pp. 1–4.

Li, S., Sankaranarayanan, S.K.R.S., Fan, C., Su, Y., Bhethanabotla, V.R., 2017. Achieving lower insertion loss and higher sensitivity in a SAW biosensor via optimization of waveguide and microcavity structures. IEEE Sens. J. 17 (6), 1608–1616.

Link, S., El-Sayed, M.A., 1999. Size and temperature dependence of the plasmon absorption of colloidal gold nanoparticles. J. Phys. Chem. B 103 (21), 4212–4217.

Liu, Y.M., Zheng, Y.L., Cao, J.T., Chen, Y.H., Li, F.R., 2008. Sensitive detection of tumor marker CA15-3 in human serum by capillary electrophoretic immunoassay with chemiluminescence detection. J. Sep. Sci. 31 (6–7), 1151–1155.

Ma, Z., Li, J., Jiang, L., Yang, M., Sui, S.-f., 2002. High sensitive DNA detection amplified by enlarging Au-nanoparticles in situ. Chem. Lett. (3), 328–329.

Mani, V., Chikkaveeraiah, B.V., Patel, V., Gutkind, J.S., Rusling, J.F., 2009. Ultrasensitive immunosensor for cancer biomarker proteins using gold nanoparticle film electrodes and multienzyme-particle amplification. ACS nano 3 (3), 585–594.

Moertel, C.G., Fleming, T.R., Macdonald, J.S., Haller, D.G., Laurie, J.A., Tangen, C., 1993. An evaluation of the carcinoembryonic antigen (CEA) test for monitoring patients with resected colon cancer. JAMA 270 (8), 943–947.

Moriizumi, T., Unno, Y., Shiokawa, S., 1987. New sensor in liquid using leaky SAW. IEEE 1987 Ultrasonics Symposium, 579–582.

Morrill, S., 2014. Combined metal-enhanced fluorescence-surface acoustic wave (MEF-SAW). Biosensor. University of South Florida, 41–60.

Nelson, R.W., Krone, J.R., Bieber, A.L., Williams, P., 1995. Mass spectrometric immunoassay. Anal. Chem. 67 (7), 1153–1158.

Ni, X.G., Bai, X.F., Mao, Y.L., Shao, Y.F., Wu, J.X., Shan, Y., Wang, C.F., Wang, J., Tian, Y.T., Liu, Q., Xu, D.K., Zhao, P., 2005. The clinical value of serum CEA, CA19-9, and CA242 in the diagnosis and prognosis of pancreatic cancer. Eur. J. Surg. Oncol. (EJSO) 31 (2), 164–169.

Ojea-Jiménez, I., Bastús, N.G., Puntes, V., 2011. Influence of the sequence of the reagents addition in the citrate-mediated synthesis of gold nanoparticles. J. Phys. Chem. C 115 (32), 15752–15757.

Onen, O., Sisman, A., Gallant, N.D., Kruk, P., Guldiken, R., 2012. A urinary Bcl-2 surface acoustic wave biosensor for early ovarian cancer detection. Sensors 12 (6), 7423–7437.

Richardson, M., Sankaranarayanan, S.K.R.S., Bhethanabotla, V.R., 2015. Low insertion loss and highly sensitive SH-SAW sensors based on 36° YX $LiTaO_3$ through the incorporation of filled microcavities. IEEE Sens. J. 15 (2), 787–796.

Rupp, S., von Schickfus, M., Hunklinger, S., Eipel, H., Priebe, A., Enders, D., Pucci, A., 2008. A shear horizontal surface acoustic wave sensor for the detection of antigen–antibody reactions for medical diagnosis. Sens. Actuators B: Chem. 134 (1), 225–229.

Schlensog, M.D., Gronewold, T.M.A., Tewes, M., Famulok, M., Quandt, E., 2004. A Love-wave biosensor using nucleic acids as ligands. Sens. Actuators B: Chem. 101 (3), 308–315.

Wanebo, H.J., Stearns, M., Schwartz, M.K., 1978. Use of CEA as an indicator of early recurrence and as a guide to a selected second-look procedure in patients with colorectal cancer. Ann. Surg. 188 (4), 481–492.

Ward, M.D., Buttry, D.A., 1990. In situ interfacial mass detection with piezoelectric transducers. Science 249 (4972), 1000–1008.

Wiggers, T., Arends, J.W., Verstijnen, C., Moerkerk, P.M., Bosman, F.T., 1986. Prognostic significance of CEA immunoreactivity patterns in large bowel carcinoma tissue. Br. J. Cancer 54 (3), 409–414.

Zhang, F., Li, S., Cao, K., Wang, P., Su, Y., Zhu, X., Wan, Y., 2015. A microfluidic love-wave biosensing device for PSA detection based on an aptamer beacon probe. Sensors 15 (6), 13839–13850.

Zhou, C., Yang, Y., Cai, H., Ren, T.-L., Chan, M., Yang, C.Y., 2013. Temperature-compensated high-frequency surface acoustic wave device. IEEE Electron Device Lett. 34 (12), 1572–1574.